Fabrication and NO₂ gas-sensing properties of reduced graphene oxide/WO₃ nanocomposite films

CrossMark

Pi-Guey Su *, Shih-Liang Peng

Department of Chemistry, Chinese Culture University, Taipei 111, Taiwan

A B S T R A C T

One-pot polyol process was combined with the metal organic decomposition (MOD) method to fabricate a room-temperature NO₂ gas sensor based on tungsten oxide and reduced graphene oxide (RGO/WO₃) nanocomposite films. Fourier Transform infrared spectrometer (FTIR), X-ray diffractometry (XRD), scanning electron microscopy (SEM) and atomic force microscopy (AFM) were used to analyze the microstructure and morphology of the fabricated films. The electrical and NO₂ gas-sensing properties of WO₃ to which various amounts of RGO were added were measured in detail as a function of concentration of NO₂ gas at room temperature, to elucidate the contribution of RGO to the NO₂ gas-sensing capacity. The NO₂ gas-sensing mechanism of the RGO/WO₃ nanocomposite films were explained by considering their composition and microstructures. The sensor that was based on a nanocomposite film of RGO/WO₃ exhibited a strong response to low concentrations of NO₂ gas at room temperature, satisfactory linearity and favorable long-term stability.

© 2014 Elsevier B.V. All rights reserved.

1. Introduction

Nitrogen oxides generated by combustion facilities and automobiles are known to be extremely harmful to the human body and are also a main cause of acid rain. Traditional, the detection of NO₂ gas has been carried out by using chemiluminescent or non-disperse infrared (NDIR) analysis. But these instruments are large, expensive and need a sampling system and complicated maintenance. Therefore, many researchers have been searching for a suitable NO₂ gas sensor for the exhaust monitoring.

Graphene consists of a two-dimensional (2D) array of carbon atoms that are covalently connected via sp2 bonds to form a honeycomb sheet [1]. Graphene exhibited intriguing properties such as high electron mobility at room temperature (250,000 cm²/Vs), exceptional thermal conductivity (5000 W m⁻¹ K⁻¹), and superior mechanical properties [2,3]. The electrical properties make it to be attractive candidates for new materials. Graphene oxide (GO) sheets have recently become attractive as possible intermediates in the manufacture of graphene [4]. In GO, carboxyl groups locate at the carbon sheet edges, and epoxy and hydroxyl functional groups decorate the surface of carbon sheets [5]. However, the oxygen functional groups of GO render it too electrically insulating for use as a conductance-based sensors. Moreover, GO can be chemically or thermally reduced to restore its conductivity several orders of magnitude by removal some of oxygen functional groups [6,7]. Therefore, reduced GO (RGO) exhibited conductive and chemically active defect sites making it an active material for sensor applications. Moreover, the RGO sheets have been used for chemiresistive sensors and exhibit great potential for gas sensing applications [8–12]. Moreover, in order to improve the sensing performance of these graphene-based sensors, the conducting polymers, metals, and metal oxides have been anchored on the surface of graphene sheets to improve the sensitivity of the resultant gas sensors [13–16].

Recently, metal oxide/graphene composite materials have attracted a great deal of attention due to potential applications in optoelectronics, energy conversion devices and gas sensors [1,17,18]. Many methods have been used to prepare metal oxide/graphene composite materials, including the hydro/solvothermal method, solution mixing method, the in-situ growth method and the photoreduction method, all of which have their own advantages and particular conditions of application [17,19–21]. Among these methods, hydro/solvothermal method is the most widely used to prepare metal oxide/graphene composite because chemical bonds form between metal oxides and graphene, which can improve the electric properties of the composite over those of the same metal oxides or graphene alone. Recently, composite films that are based on WO₃ nanopowders and graphene have been reported to be as new gas-sensitive materials to reduce further the operating temperature and to improve the sensitivity of sensors based on these materials [22,23]. Yu et al. fabricated WO₃ nanorodes/graphene nanocomposites using the hydrothermal

---

* Corresponding author: Tel.: +886 2 28610511x25332; fax: +886 2 28614212.
E-mail address: spg@faculty.pccu.edu.tw (P.-G. Su).

method for sensing NO_2 [22]. Senguttuvan et al. fabricated a more rapidly responding NO_2 gas sensor based on WO_3/graphene nanocomposites that were made by the hydrothermal method [23]. The sensing characteristics of these WO_3/graphene-based NO_2 gas sensors depend on their microstructure, which are determined by their fabrication process. Most NO_2 gas sensors have been fabricated by synthesizing graphene that is decorated with WO_3 nanomaterial and drop-coating it on a substrate.

Polyol-based synthesis route has been used for preparing nano-metal oxide materials, because the reaction conditions are easily established, and yield nano-sized particles in the form of dimensionally stable colloidal suspensions. Briefly, this approach uses a polyol with a high boiling point, including diethylene glycol, glycerol, glycol and others, as the reaction medium in the preparation of oxide materials. The polyols act as stabilizers, limiting particle growth and prohibiting agglomeration. Therefore, suitable reactants from homogenous solution (metal acetates/chlorides/alkoxides) are hydrolyzed at elevated temperature, forming nano metal oxides/precursors in suspension in polyol [24–26]. Additionally, the metal organic decomposition (MOD) method for depositing a metal oxide thick film is easily and inexpensively applied [27,28]. Briefly, a metal alkoxide is spin-coated on a substrate, and then MOD forms a strongly adhesive and homogeneous film of metal oxide. Tsai et al. [29–31] used the MOD method to prepare a SnO_2 film to detect amounts of alcohol and CO gases. No attempt has been made to fabricate an NO_2 gas sensor that is based on RGO/WO_3 nanocomposite films by combining the one-pot polyol process with the MOD method. Additionally, the pure WO_3 film typically must usually be used at temperatures from 200 to 500 °C [32,33]. To improve the high resistance and weak response of the WO_3 film operating at room-temperature for practical use, nanocomposite films of RGO and WO_3 were fabricated in this study by such a combination of methods. These films have the advantages of being highly effective, inexpensive and suitable for industrial for mass production. The key step in the fabrication of the RGO/WO_3 nanocomposite film was that the reduction of GO to RGO and the conversion of WO_3 nanoparticles from H_2WO_4 precursors were produced simultaneously in the one-pot polyol approach. The structural characteristics of the RGO/WO_3 nanocomposite films were investigated by X-ray diffraction (XRD) and Fourier Transform infrared spectrometer (FTIR). The surface characteristics of the RGO/WO_3 nanocomposite films were observed using atomic force microscopy (AFM) and scanning electron microscopy (SEM). The NO_2 sensing performance of RGO/WO_3 nanocomposite films with various amounts of the RGO loaded into the WO_3 matrix was studied as the function of concentration of NO_2 gas at room-temperature. Differences in the composition and microstructure were adopted to explain the effect of adding RGO on the sensing mechanism of the RGO/WO_3 nanocomposite films.

2. Experimental

2.1. Preparation of GO

GO was prepared from natural graphite by the Hummers method [34]. Briefly, 0.5 g graphite powder was reacted with a mixture of 2 g $NaNO_3$, 12 mL concentrated H_2SO_4 and 3 g $KMnO_4$; then 40 mL deionized water (DIW) and 10 mL H_2O_2 (30%) were added. The product was filtered and washed with 5% HCl solution and deionized water to yield a brown power. An exfoliated aqueous GO dispersion was produced after sonication for 2 h. The resultant mixture was filtered and washed with DIW by centrifuging until the solution attained a pH of 6, and was then

sonicated to form a stable suspension of GO in aqueous media. The resulting aqueous GO solution had a concentration of 0.85 mg/mL.

2.2. Fabrication of gas sensors based on WO_3 films

Fig. 1 displays a picture of the structure of NO_2 sensors fabricated on an alumina substrate. The interdigited gold electrodes were made by screen printing. The electrode gap was 0.2 mm. Tungstic acid (H_2WO_4) (3.0 g) (99.9%, 5.59 g/cm³, Merck) was added to 10 g of glycerol (99.5%, 1.259 g/cm³, Merck) and the solution was heated to 190 °C for 1 h with vigorous magnetic stirring. The reaction can be easily followed by observing its distinctive color changes. Within minutes after the reaction's reaching 190 °C, the yellow solution turned pale green and then slowly changed to a deep blue suspension, indicating the formation of tungsten oxide nanoparticles in glycerol. The blue precursor was spin-coated on an alumina substrate with a pair of comb-like electrodes. Then, it was dried by heating to 170 °C in air for 2 h; MOD was then performed in a furnace at 500 °C for 4 h in the ambient atmosphere to form a film of WO_3. During the MOD process, the temperature was increased from the ambient temperature to 500 °C at a heating rate of 5 °C/min. Therefore, a gas sensor based on WO_3 film was obtained (Fig. 1).

2.3. Fabrication of gas sensors based on RGO/WO_3 nanocomposite films

The RGO/WO_3 nanocomposites were synthesized as follows. Tungstic acid (H_2WO_4) (3.0 g) and the required amounts of GO were added to 10 g of glycerol and the resultant solution was heated to 190 °C for 1 h with vigorous magnetic stirring. The solution was continuously stirred until a stable suspension was obtained. The level of doping with GO was varied among 1.6 wt%, 3.2 wt% or 11.8 wt% (of H_2WO_4). The RGO/WO_3 nanocomposite films were formed by MOD in the same manner as used in the fabrication of a gas sensor based on a WO_3 film. For fabricating the RGO/WO_3 nanocomposite films, an MOD temperature of 500 °C was maintained for 4 h.
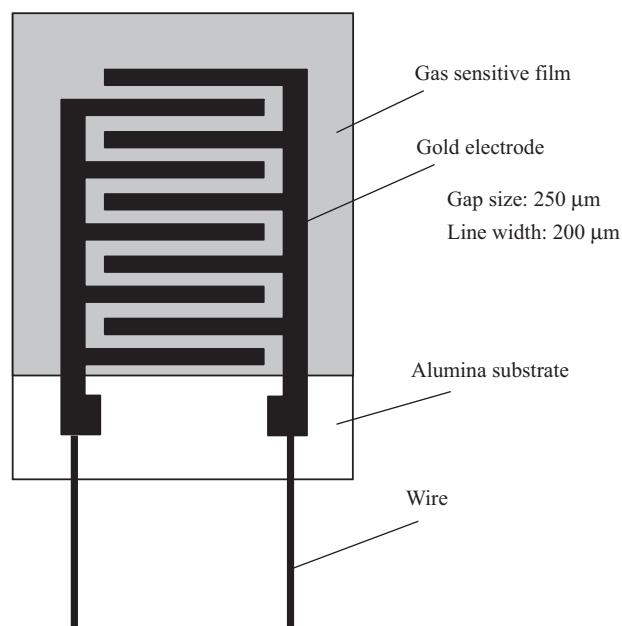
Fig. 1. Structure of NO_2 gas sensor.

2.4. Instruments and analysis

A Fourier Transform infrared spectrometer (FTIR, Nicolet 380) was used to obtain the IR spectra of the GO and RGO. The surface microstructure of the WO_3 film and RGO/WO_3 nanocomposite films coated on an alumina substrate was investigated using a field emission scanning electron microscope (FEI company, Nova Nano-SEM™ 230) quipped with an energy dispersive spectrometer (EDS) and an atomic force microscope (AFM, Ben-Yuan, CSPM 4000) in tapping mode which the horizontal and vertical resolution are 0.26 and 0.10 nm, respectively. The XRD powder pattern of the WO_3, GO and RGO/WO_3 nanocomposite films were measured using Cu K_α radiation (Shimadzu, Lab XRD-6000). The electrical and sensing characteristeristics were measured using a static state system at room temperature, as shown in Fig. 2. Each sensor was connected in series with a load resistor and a fixed 5V tension (DC mode) was continuously supplied to the sensor circuit from a power supply (GW, PST-3202). The resistance of the sensor was determined from the voltage at the ends of the load resistor using a DAQ device (NI, USB-6218) in various concentrations of gas. The standard NO_2, NH_3, and H_2S gases were purchased from Shen Yi Gas Co. (Taiwan). The concentration for standard NO_2, NH_3, and H_2S gases were 100,000, 1000 and 1000 ppm, respectively. The required various gas concentrations were produced by diluting the known volume of standard gas with dry air and then were injected into the chamber. The desired various gas concentrations were measured using a calibrated gas sensor system (Dräger, Mini-Warn). The interfering experiment was performed by measuring the resistance of the sensor exposure to NH_3, H_2S and H_2O gases, respectively. The volume of the chamber is 18 l. The gas inside the chamber was uniformly distributed using a fan. After some time, the chamber was purged with air and the experiment was repeated for another cycles. All experiments were performed at room temperature, which was about 23.0 ± 1.5 °C and the relative humidity was 40% RH.

3. Results and discussion

3.1. Preparation and structural characteristics of RGO/WO_3 nanocomposite films

3.1.1. IR spectra

GO was used as the precursor to prepare the RGO/WO_3 nanocomposite was prepared by the one-pot polyol reaction of H_2WO_4 in glycerol because that the GO had hydrophilic property to be homogenously dispersed in a H_2WO_4 matrix and easily reduced to RGO. To confirm the feasibility of the polyol method for reducing GO to RGO in the one-pot polyol synthesis of RGO/WO_3 nanocomposite, GO was the first reduced in the absence of H_2WO_4 in glycol. The IR spectrum of the GO in Fig. 3(a) includs a peak at 3350 cm^{-1} attributable to the O–H stretching vibration, peaks at 1740 and 1630 cm^{-1} attributable to the C=O stretching vibrations, and a peak at 1357 cm^{-1} attributable to the deformation of O–H. The one-pot polyol synthesis process reduced the heights of the peaks at 1740, 1630 and 1357 cm^{-1} (Fig. 3(b)), suggesting the successful reduction of GO in the one-pot polyol reaction. Therefore, partially reduced GO was formed in the RGO/WO_3 nanocomposite. Additionally, W(VI) was partially reduced to W(V) in polyol to yield a deep blue non-stoichiometric precursor because W(VI) is a moderate oxidizing agent [35]. Therefore, polyol acted as a reducing agent for W(VI), and GO was simultaneously reduced to RGO in the one-pot polyol reaction of H_2WO_4. Additionally, no new peak was observed from the RGO/WO_3 samples, indicating that no new bonding formed between the RGO and WO_3 matrix.
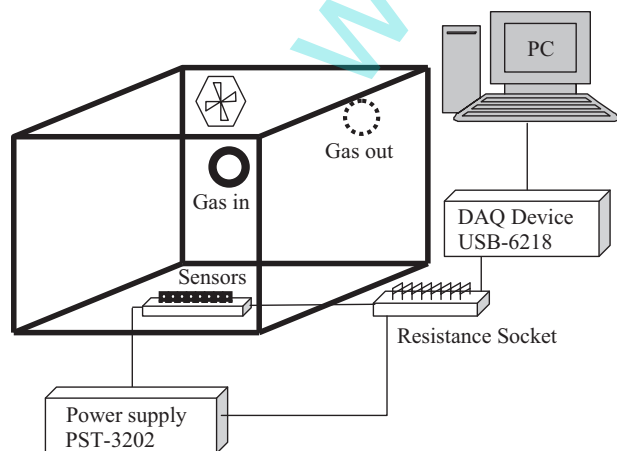
3.1.2. XRD characterization

Fig. 4 shows the XRD spectra of the GO, WO_3 film and RGO/WO_3 nanocomposite films that were prepared by the combined one-pot polyol and MOD method. For GO, a sharp diffraction peak (002) appears at 10.75°, which indicates that most of the graphite powder was oxidized into GO by expanding d-spacing of 6.70 Å [36]. The XRD patterns of WO_3 film show three main peaks at $2\theta = 23.1$, 23.6 and 24.3°, which are identified as corresponding to (002), (020) and (200) orientations, respectively. The XRD patterns showed the formation of monoclinic WO_3, as in the Joint
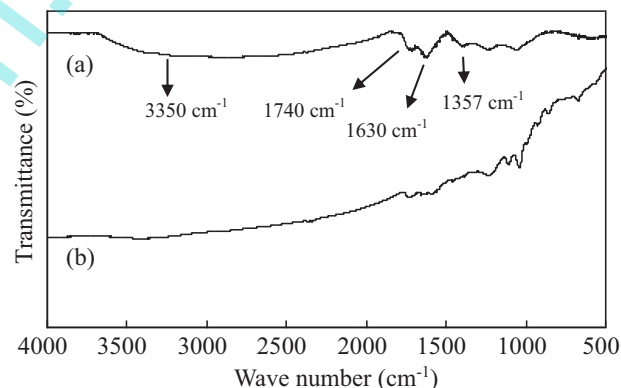
Fig. 3. IR spectra of (a) GO and (b) RGO was fabricated by one-pot polyol process.

Fig. 2. Measurement system for testing gas sensors.
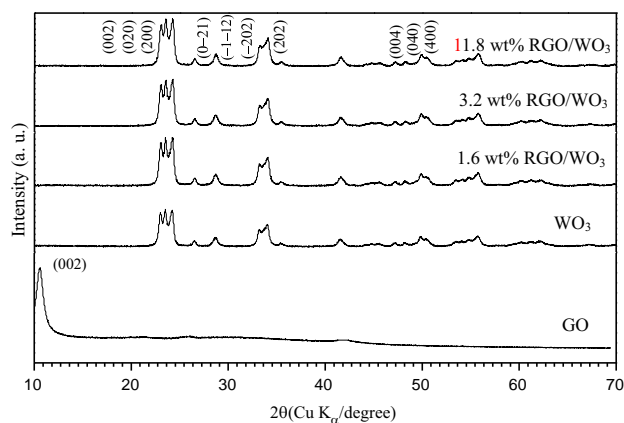
Fig. 4. XRD patterns of WO_3 film and RGO/WO_3 nanocomposite films that were fabricated by one-pot polyol process and MOD at 500 °C for 4 h.

Table 1
Crystallite size of RGO/WO₃ prepared by one-pot polyol process combined with MOD at 500 °C.

Sample	Crystallite size (nm)
WO₃	61.59
1.6 wt% RGO/WO₃	61.60
3.2 wt% RGO/WO₃	61.61
11.8 wt% RGO/WO₃	61.61

Committee of Powder Diffraction Standards (JCPDS 00-020-1324) [37]. For the RGO/WO₃ nanocomposite, by increasing the doping amount of GO in the precursor solution from 1.6 to 11.8 wt%, the XRD patterns showed no appreciable difference between the orientations and phases of WO₃ and RGO/WO₃ samples, probably due to the reduction of GO by glycerol or RGO was embedded in the WO₃ matrix and so could not be easily detected by X-ray diffraction. The crystallite size of WO₃ and RGO/WO₃ samples after MOD at 500 °C for 4 h was estimated from XRD peaks according to Scherrer's equation,

$$D = \frac{0.9\lambda}{(B \cos \theta)} \tag{1}$$

where D represents mean grain size; B represents the full width at half maximum of the peak; λ is the wavelength of the X-rays, and θ is the angle of the center of the peak. The crystallite size was estimated from the half width of the (200) peak. Table 1 shows the estimated sizes of the crystallite of the WO₃ and RGO/WO₃ samples. By increasing the doping amount of GO in the precursor solution from 1.6 to 11.8 wt%, no appreciable difference between the crystallite size of WO₃ and RGO/WO₃ samples was observed.

3.1.3. AFM and SEM analyses

Fig. 5 presents the surface morphology of the WO₃ film and 3.2 wt% RGO/WO₃ nanocomposite film that were prepared by the combined one-pot polyol and MOD method, determined using tapping-mode AFM. The size of each image is 5 μm × 5 μm. Both WO₃ film (Fig. 5(a)) and 3.2 wt% RGO/WO₃ nanocomposite film (Fig. 5(b)) exhibited a uniform granular morphology. The surface roughness of the WO₃ film and 3.2 wt% RGO/WO₃ nanocomposite film were 21.2 and 19.2 nm, respectively. Fig. 6 presents SEM images and EDS spectra of the WO₃ film and 3.2 wt% RGO/WO₃ nanocomposite film that were prepared by the combined one-pot polyol and MOD method. Both WO₃ film (Fig. 6(a)) and 3.2 wt% RGO/WO₃ nanocomposite film (Fig. 5(b)) exhibited a flat surface. In Fig. 6(b), a local dark region was clearly observed. Comparing the EDS spectra of the WO₃ film and the 3.2 wt% RGO/WO₃ nanocomposite film reveals that the RGO was doped into the WO₃ matrix. Additionally, no naked RGO was present on the surface of the RGO/WO₃ nanocomposite film, even when the amount of added RGO was 11.8 wt%.

3.2. Electrical and Gas sensing properties of RGO/WO₃ nanocomposite films

3.2.1. Effect of RGO content on the electrical properties and sensing mechanism

The sensor response (S) was calculated by the following equation:

$$S(\%) = \frac{(R_{gas} - R_{air})}{R_{air}} \times 100\% = \frac{(\Delta R)}{R_{air}} \times 100\% \tag{2}$$

where R_{gas} and R_{air} are the electrical resistances of the sensor in the tested gas and air, respectively. Fig. 7 plots the responses of the sensors that were based on WO₃ film and RGO/WO₃ nanocomposite films that were prepared using various amounts of GO, to
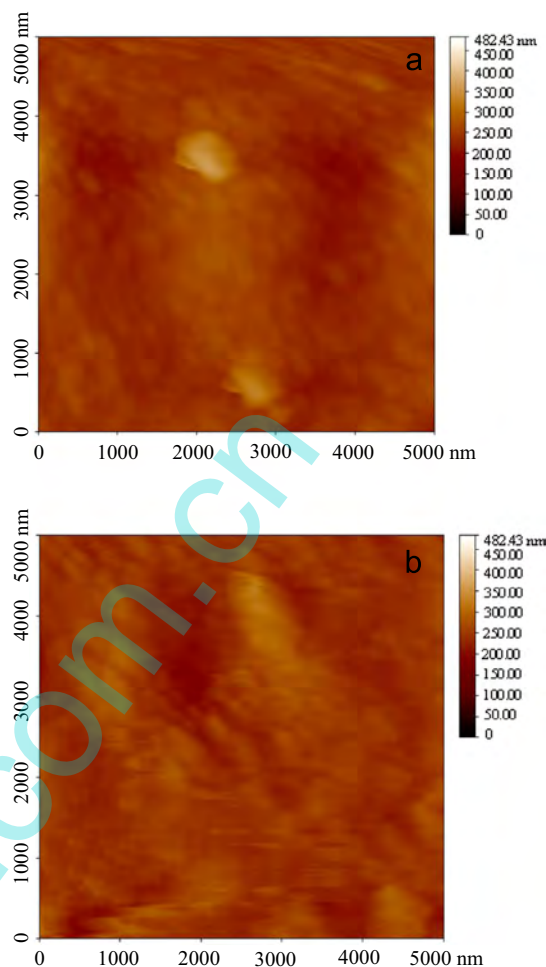
Fig. 5. AFM images of (a) WO₃ film and (b) 3.2 wt% RGO/WO₃ nanocomposite film that were fabricated by one-pot polyol process and MOD at 500 °C for 4 h.

various concentrations of NO₂ gas at room temperature. Clearly, the responses (S) of the sensors that were made of the RGO/WO₃ nanocomposite films were significantly stronger than that of the sensor that was made of the pure WO₃ film. When the amount of RGO added was below 3.2 wt%, the response (S) of the sensors increased and the concentration of NO₂ gas-sensing increased with increasing the amount of RGO added. However, when the mass of RGO added was increased to 11.8 wt%, the RGO/WO₃ nanocomposite film exhibited a small response (S) in the NO₂ gas range studied. When less than 3.2 wt% of RGO were added, as described in Section 3.1.3, the surface morphology of the WO₃ film did not obviously differ from that of the RGO/WO₃ nanocomposite film. Additionally, BET analysis reveals that the difference between the surface area of WO₃ and RGO/WO₃ films was very small. Therefore, differences in surface morphology may not be directly responsible for the improved in the NO₂ gas-sensing of the RGO/WO₃ nanocomposite films compared to that of the pure WO₃ film. Therefore, two main effects are proposed to the improvement in the response (S) of the sensors of the WO₃ film doped with RGO. First, the resistance of pure WO₃ film was around 800 kΩ. When the doping amount of RGO was 1.6 wt%, the resistance of the RGO/WO₃ nanocomposite film was reduced to ∼98 kΩ. When the doping amount of RGO was increased to 3.2 wt%, the resistance of the RGO/WO₃ nanocomposite film was reduced further to ∼9 kΩ. Therefore, revealing that the added GO was reduced to conductive RGO which formed new electrical paths in the WO₃ matrix in the one-pot polyol reaction. In this situation, a new conductive path was formed by the embedded RGO, and thus the
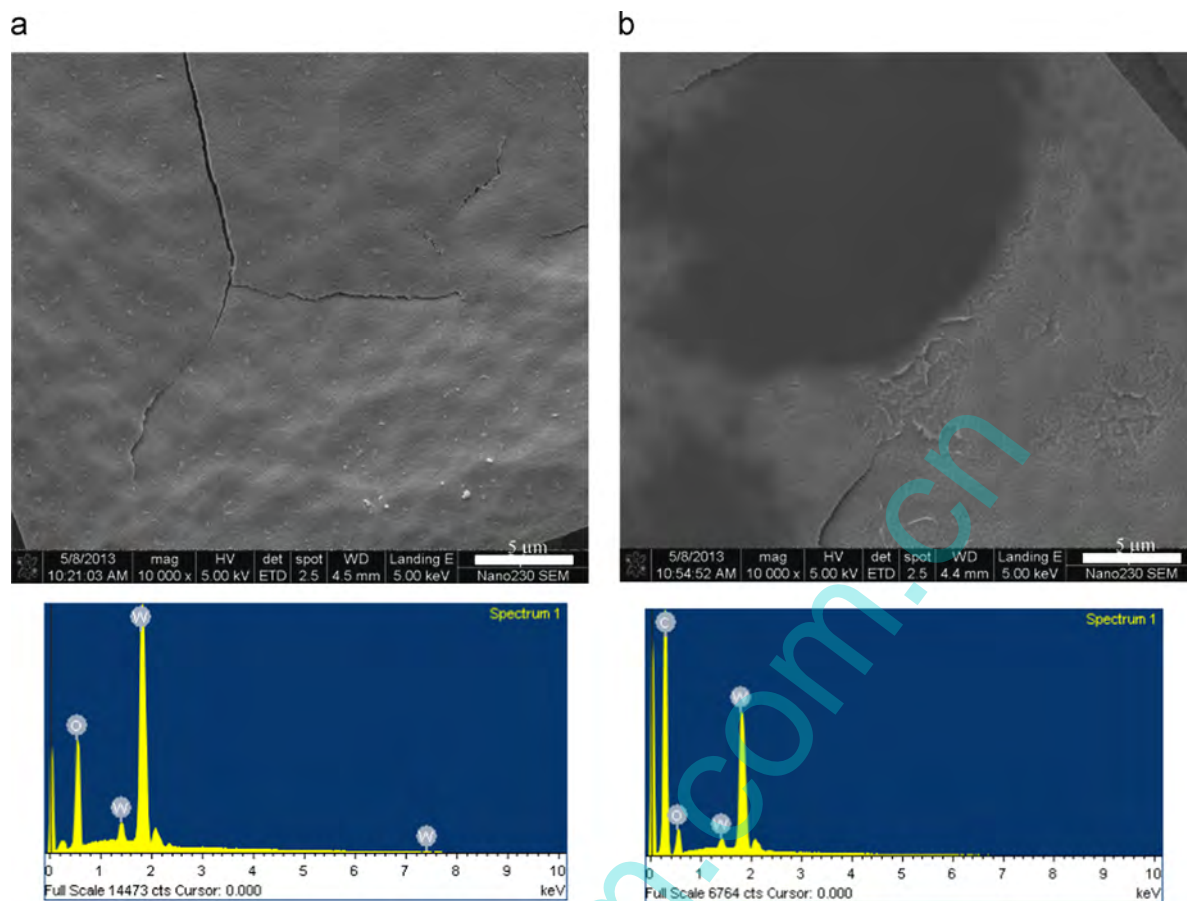
Fig. 6. FE-SEM images and EDS spectra of (a) WO_3 film and (b) 3.2 wt% RGO/WO_3 nanocomposite film that were fabricated by one-pot polyol process and MOD at 500 °C for 4 h.
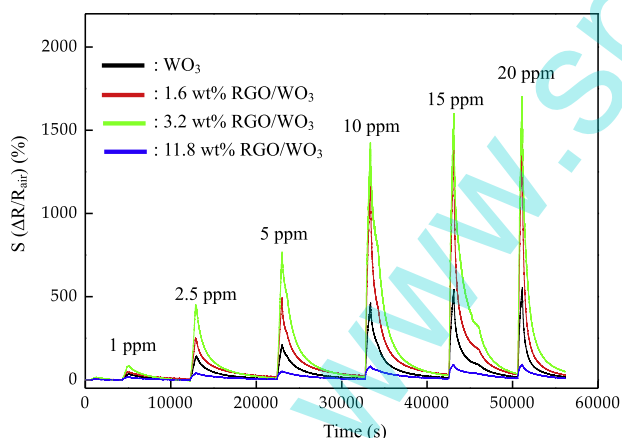
Fig. 7. Response (S) of NO_2 gas sensors based on RGO/WO_3 nanocomposite films that were prepared by one-pot polyol process and MOD at 500 °C for 4 h with various amounts of added RGO, as function of time (s) for various concentrations of NO_2 gas at room temperature.

Fig. 8. Equivalent cross-sectional views of a NO_2 gas sensor based on RGO/WO_3 nanocomposite film with hetero-structure (Au/n-WO_3/p-RGO/n-WO_3/Au).

sensitivity of the RGO/WO_3 nanocomposite film was better than that of the WO_3 film. When the amount of added RGO was increased to 11.8 wt%, the amount of added RGO exceeded the percolation threshold so that the change in conductance of the sensing material due to adsorption of NO_2 gas molecules was not obvious. Second, the WO_3 behaved as an n-type semiconductor, and RGO behaved as a p-type semiconductor. Therefore, from the results of XRD and SEM analyses, the WO_3 matrix surrounds the RGO, the p–n hetero-junction that was formed by WO_3 and RGO, as presented in Fig. 8. This hetero-structure was associated with

the co-existence of two depletion layers (and associated potential barriers). The first depletion layer was located at the surface of the WO_3 film and the second was at the interface between the RGO and the WO_3 film. Therefore, the p–n heterojunctions were responsible for the fact that the sensor that was based on WO_3/RGO nanocomposite film was much more sensitive than that based on WO_3 film [38,39]. Therefore, the RGO/WO_3 nanocomposite film easily detected the gas at room temperature, owing to the effects of by the combination of the percolation effect and its hetero-structure.

3.2.2. Gas-sensing properties

Fig. 9 plots the responses (S) of the sensor that was made of the 3.2 wt% RGO/WO_3 nanocomposite film to various concentrations of NO_2. The sensor had a response of 16.8% even at a low NO_2 testing concentration of 0.5 ppm. Therefore, the NO_2 gas sensor that was made of the RGO/WO_3 nanocomposite film that was doped with 3.2 wt% of RGO was chosen to study further its other
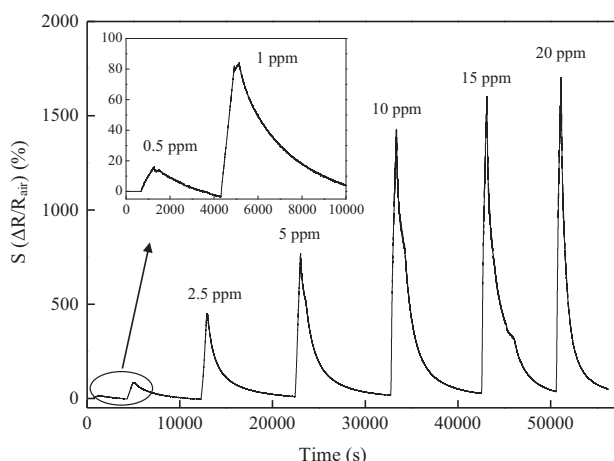
Fig. 9. Response (S) of NO_2 gas sensors based on 3.2 wt% RGO/WO_3 nanocomposite film, as function of time (s) for various concentrations of NO_2 gas at room temperature.
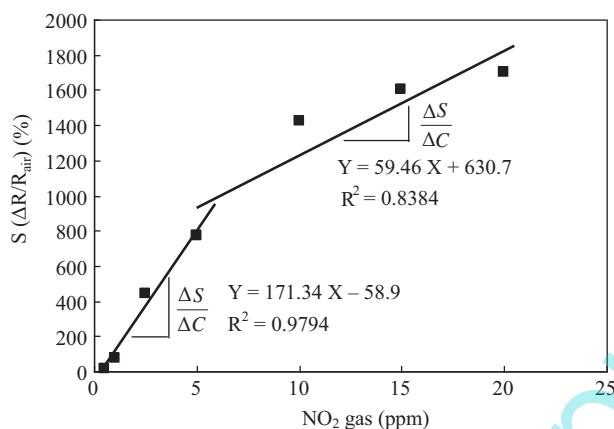
Fig. 10. Linear dependence of response of NO_2 gas sensor based on 3.2 wt% RGO/WO_3 nanocomposite film that was fabricated by one-pot polyol process and MOD at 500 °C for 4 h on concentration of NO_2 gas at room temperature. Sensitivity ($\Delta S/\Delta C$) is determined from the slope of the linear curve.
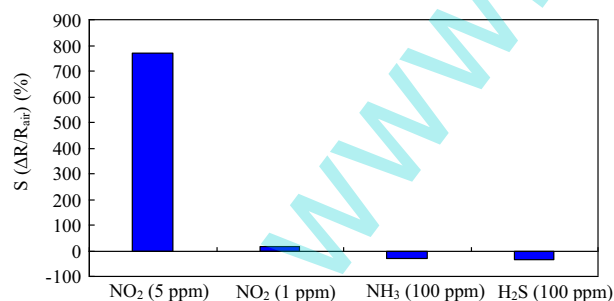
Fig. 11. Response (S) of NO_2 gas sensors based on (a) RGO/WO_3 nanocomposite films that were prepared by one-pot polyol process and MOD at 500 °C for 4 h to various gases.

gas sensing properties. Fig. 10 plots the response (S) as a function of concentration of NO_2 gas for the sensor that was made of the 3.2 wt% RGO/WO_3 nanocomposite film. The sensitivity ($\Delta S/\Delta C$) is determined from the slopes of the plots of response vs. gas concentration. A steep decrease in the slope was observed at from 5 to 20 ppm of NO_2 gas. Therefore, the sensitivity at 0.5 to 5 ppm NO_2 gas was higher than that at 5 to 20 ppm. Fig. 11 plots the results concerning the interfering effects of NH_3 and H_2S gases on the NO_2 gas sensor. NH_3 and H_2S gases may be regarded as having unobvious interference effects with NO_2 at a testing NO_2

concentration of 5 ppm. However, NH_3 and H_2S gases may be regarded having interference effects with NO_2 at a testing NO_2 concentration under 1 ppm. Additionally, from the results in Fig. 11, the sign of the response (S) for the considered adsorbates can be understood as indicating one of two charge transfer mechanisms. In this work, NO_2 doped the RGO/WO_3 film with holes, while NH_3 and H_2S doped it with electrons. Accordingly, the prepared RGO/WO_3 film exhibited the electrical behavior of an n-type semiconductor. During the sensing process, the adsorption of electron-withdrawing NO_2 molecules compensates for the hole carriers in the n-type RGO/WO_3, causing the electrical resistance of the RGO/WO_3 nanocomposite film to increase with concentration of NO_2. The electrical resistance of the RGO/WO_3 nanocomposite film decreased when the film was exposed to NH_3 and H_2S gases because NH_3 and H_2S are electron-donating gases. Fig. 12 plots the effect of ambient humidity on the response (S) of the NO_2 gas
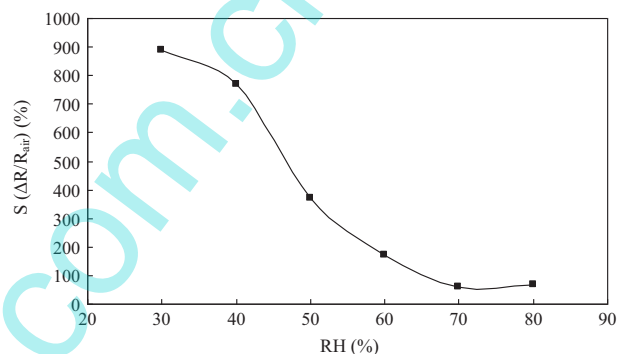
Fig. 12. Effect of ambient humidity on response of the NO_2 gas sensor based on 3.2 wt% RGO/WO_3 nanocomposite film that was fabricated by one-pot polyol process and MOD at 500 °C for 4 h to 5 ppm of NO_2 gas at room temperature.
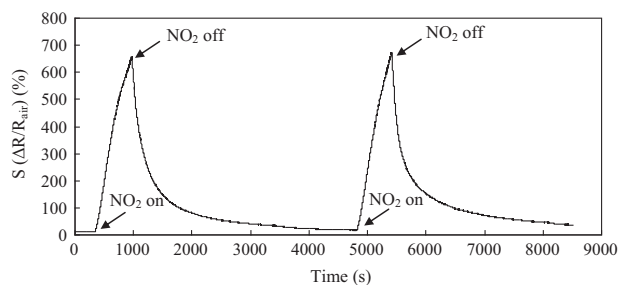
Fig. 13. Reproducibility of response of NO_2 gas sensor based on 3.2 wt% RGO/WO_3 nanocomposite film that was fabricated by one-pot polyol process and MOD at 500 °C for 4 h to 5 ppm of NO_2 gas at room temperature.
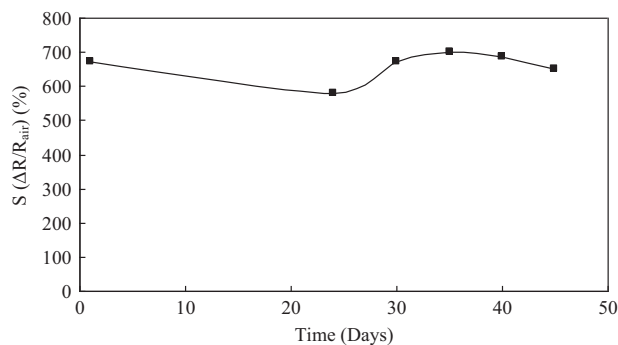
Fig. 14. Long-term stability of response of the NO_2 gas sensor based on 3.2 wt% RGO/WO_3 nanocomposite film that was fabricated by one-pot polyol process and MOD at 500 °C for 4 h in 5 ppm of NO_2.

Table 2
Comparison of performance of NO_2 gas sensor developed herein with the literature.

Sensing material	Fabrication method	Response (%)	Response/recovery times	References
RGO/WO_3 nanocomposite	one-pot polyol process combined with MOD	769[a]	9/18 min	This work
WO_3 nanorods decorated on graphene	hydrothermal method	202[b]	–[c]	[22]
WO_3/RGO nanocomposite	hydrothermal method	135[d]	25/200 s	[23]
MWCNTs/WO_3 nanocomposite	one-pot polyol process combined with MOD	77[e]	10.5/20	[39]

[a] The sensor in response to 5 ppm NO_2 gas at room temperature.
[b] The sensor in response to 20 ppm NO_2 gas at 300 °C.
[c] No explanation in the literature.
[d] The sensor in response to 5 ppm NO_2 gas at 250 °C.
[e] The sensor in response to 5 ppm NO_2 gas at room temperature.

sensor at a testing NO_2 concentration of 5 ppm. The response (S) of the NO_2 gas sensor decreased as the ambient humidity increased, because the physisorbed water occupied the active sites of the sensing materials. Fig. 13 plots the real-time response of the NO_2 gas sensor at a testing concentration of NO_2 of 5 ppm. The response of the sensor increases significantly when the NO_2 gas was introduced into the chamber. However, we did not observe the saturated state of the NO_2 gas sensor, even when the exposure time was prolonged to 10 min. Additionally, two gas on/off cycles produced similar responses, indicating that the NO_2 gas sensor exhibited excellent reproducibility even when the exposure time was prolonged to 10 min. Therefore, we defined the exposure time of about 10 min as the effective response time for the NO_2 gas sensor. The recovery time is defined as the time required for the sensor to recover 90% of the decrease in resistance after the sensor is exposed to a dry gas. The recovery time of the NO_2 gas sensor was 18 min at a testing concentration of NO_2 of 5 ppm. Fig. 14 plots the long-term stability. The response (S) of the NO_2 gas sensor did not significantly vary for at least 45 days in a testing NO_2 concentration of 5 ppm. Table 2 compares the NO_2 gas sensing properties of the NO_2 gas sensor proposed herein with those of sensors in our previous work [39] and elsewhere in the literatures [22,23]. The response of the NO_2 gas sensor that was proposed herein was stronger than that of the NO_2 gas sensor that was fabricated by the hydrothermal method. Additionally, the NO_2 gas sensor that was made of RGO/WO_3 nanocomposite film exhibited higher response than that of the NO_2 gas sensor made of MWCNTs/WO_3 nanocomposite film because that the RGO had high electron mobility, favoring the transport process of electron easily in the RGO/WO_3 nanocomposite film at room temperature [2]. However, the response/recovery times of the NO_2 gas sensor that was proposed herein were longer than that of the NO_2 gas sensor that was fabricated by the hydrothermal method, perhaps because the former sensor had a compact sensing-film.

4. Conclusions

RGO/WO_3 nanocomposite film was fabricated on an alumina substrate by combining the one-pot polyol process with the MOD method. It was found that the introduction of RGO was effective for increasing the conductance of RGO/WO_3 nanocomposite film especially at low concentration of NO_2 gas. Therefore, the response of the RGO/WO_3 nanocomposite film to NO_2 gas increased dramatically when a few RGO was added to the WO_3 film. However, the amount of RGO added exceeded the percolation threshold, no variation in response versus concentration of NO_2 gas was clearly observed.

The NO_2 gas sensor that was based on a RGO/WO_3 film that was doped with 3.2 wt% of RGO responded more strongly than any of the tested sensors that were based on such films with different degrees of doping. The NO_2 gas sensor was very sensitive with

acceptable linearity ($Y = 171.34 X - 58.9$; $R^2 = 0.9794$) between 0.5 and 5 ppm, good reversibility and long-term stability (at least 45 days) when used at room temperature. NH_3 and H_2S gases may be regarded as having unobvious interference effects with NO_2 at a testing NO_2 concentration of 5 ppm. Ambient humidity significantly affected the NO_2 gas sensor. The response and recovery times were 9 and 18 min, respectively.

References

[1] K.S. Novoselov, A.K. Geim, S.V. Morozov, D. Jiang, Y. Zhang, S.V. Dubonos, I.V. Grigorieva, A.A. Firsov, Science 306 (2004) 666–669.
[2] K.S. Novoselov, A.K. Geim, S.V. Morozov, D. Jiang, M.I. Katsnelson, I.V. Grigorieva, S.V. Dubonos, A.A. Firsov, Nature 438 (2005) 197–200.
[3] A.A. Balandin, S. Ghosh, W. Bao, I. Calizo, D. Teweldebrhan, F. Miao, C.N. Lau, Nano Lett. 8 (2008) 902–907.
[4] C. Daniela, V.D. Marcano, J.M. Kosynkin, J.M. Berlin, A. Sinitskii, Z. Sun, A. Slesarev, L.B. Alemany, W. Lu, M.J.M. Tour, Nano 4 (2010) 4806–4814.
[5] A. Lerf, H. He, M. Forster, J. Kilnowski, J. Phys. Chem. B 102 (1998) 4477–4482.
[6] S.F. Pei, H.M. Cheng, Carbon 50 (2012) 3210–3228.
[7] G. Lu, L.E. Ocola, J. Chen, Appl. Phys. Lett. 94 (2009) 083111-3.
[8] J.T. Robinson, F.K. Perkins, E.S. Snow, Z. Wei, P.E. Sheehan, Nano. Lett. 8 (2008) 3137–3140.
[9] V. Dua, S.P. Surwade, S. Ammu, S.R. Agnihotra, S. Jain, K.E. Roberts, S. Park, R.S. Ruoff, S.K. Manohar, Angew. Chem. Int. Ed. 49 (2010) 2154–2157.
[10] N. Hu, Y. Wang, J. Chai, R. Gao, Z. Yang, E.S.W. Kong, Y. Zhang, Sens. Actuators B 163 (2012) 107–114.
[11] Z. Yang, R. Gao, N. Hu, J. Chai, Y. Cheng, L. Zhang, H. Wei, E.S.W. Kong, Y. Zhang, Nano-Micro Lett. 4 (2012) 1–9.
[12] N. Hu, Z. Yang, Y. Wang, L. Zhang, Y. Wang, X. Huang, H. Wei, L. Wei, Y. Zhang, Nanotechnology 25 (2014) 025502.
[13] X. Huang, N. Hu, R. Gao, Y. Yu, Y. Wang, Z. Yang, E.S.W. Kong, H. Wei, Y. Zhang, J. Mater. Chem. 22 (2012) 22488–22495.
[14] A. Gutés, B. Hsia, A. Sussman, W. Mickelson, A. Zettl, C. Carraro, R. Maboudian, Nanoscale 4 (2012) 438–440.
[15] Q. Huang, D. Zeng, H. Li, C. Xie, Nanoscale 4 (2012) 5651–5668.
[16] P.A. Russo, N. Donato, S.G. Leonardi, S. Baek, D.E. Conte, G. Neri, N. Pinna, Angew. Chem. Int. Ed. 51 (2012) 11053–11057.
[17] J. Chen, J. Shi, X. Wang, H. Cui, M. Fu, Chin. J. Catal. 34 (2013) 621–640.
[18] S. Bai, X.P. Shen, RSC Adv. 2 (2012) 64–98.
[19] Y. Si, E.T. Samulski, Chem. Mater. 20 (2008) 6792–6797.
[20] J.W. Qin, M.H. Cao, N. Li, C.W. Hu, J. Mater. Chem. 21 (2011) 17167–17174.
[21] T.S. Wu, S. Liu, Y.L. Luo, W.B. Lu, L. Wang, X.P. Sun, Nanoscale 3 (2011) 2142–2144.
[22] X. An, J.C. Yu, Y. Wang, Y. Hu, X. Yu, G. Zhang, J. Mater. Chem. 22 (2012) 8525–8531.
[23] S. Srivastava, K. Jain, V.N. Singh, S. Singh, N. Vijayan, N. Dilawar, G. Gupta, T.D. Senguttuvan, Nanotechnology 23 (2012) 205501.
[24] C. Feldmann, Scr. Mater. 44 (2001) 2193–2196.
[25] C. Feldmann, C. Metzmacher, J. Mater. Chem. 11 (2001) 2603–2606.
[26] C. Feldmann, Adv. Funct. Mater. 2 (2003) 101–107.
[27] G.M. Vest, Mater. Res. Soc. Symp. Proc. 60 (1986) 35.
[28] P. Van Geloven, J. Moons, M. Honore, J. Roggen, Sens. Actuators 17 (1989) 361.
[29] P.P. Tsai, I.C. Chen, M.H. Tzeng, MRL Bull. Res. Dev. 6 (1992) 67–72.
[30] P.P. Tsai, I.C. Chen, M.H. Tzeng, Sens. Actuators B 13–14 (1993) 610–612.
[31] P.P. Tsai, I.C. Chen, M.H. Tzeng, Tin oxide (SnOx) carbon monoxide sensor fabricated film methods, Sens. Actuators B 24–25 (1995) 537–539.

[32] H.T. Sun, C. Cantalini, L. Lozzi, M. Passacantando, S. Santucci, M. Pelino, Thin Film Devices, Sensors and Actuators, Thin Solid Films 287 (1996) 258–265.
[33] Y.G. Choi, G. Sakai, K. Shimanoe, N. Miura, N. Yamazoe, Sens. Actuators B 95 (2003) 258–265.
[34] W.S. Hummers, R.E. Offeman, J. Am. Chem. Soc. 80 (1958) 1339.
[35] P. Porkodi, V. Yegnaraman, D. Jeyakumar, Mater. Res. Bull. 41 (2006) 1476–1486.
[36] A.B. Bourlinos, D. Gournis, D. Petridis, T. Szabó, A. Szeri, I. Dékány, Langmuir 19 (2003) 6050–6055.
[37] ⟨http://www.icdd.com/products/overview.htm⟩.
[38] B.Y. Wei, M.C. Hsu, P.G. Su, H.M. Lin, R.J. Wu, H.J. Lai, Sens. Actuators B 101 (2004) 81–89.
[39] P.G. Su, T.T. Pan, Mater. Chem. Phys. 125 (2011) 351–357.